COAL WORKING FACE IMAGING BY SEISMIC INTERFEROMETRY - USING CONVEYER BELT NOISE AS SOURCE

BIN LU and JIAXING FENG

CCTEG Xi'an Research Institute, Xi'an 710077, P.R. China. lubin2000@163.com

(Received January 5, 2016; revised version accepted July 17, 2017)

ABSTRACT

Lu, B. and Feng, J., 2017. Coal working face imaging by seismic interferometry - using conveyer belt noise as source. *Journal of Seismic Exploration*, 26: 411-432.

The real-time monitoring of stress conditions around the working faces of coal mines has been found to be an effective method to prevent geological disasters, such as roof collapses and water bursts. In this research study, a seismic interferometry method was proposed based on conveyor belt noise, for the purpose of implementing working face real-time imaging. In order to examine the seismic interferometry induced by conveyor belt noise, a stationary phase integration analysis of the cross-correlation of the thread seismic source was first conducted. Then, a numerical simulation of the discrete linear array noise traces was discussed. The analysis showed that the seismic interferometry of the thread seismic sources produced some fake events, which were observed prior to the true events. Therefore, the arrival-time of true events could be picked up by using a simple cross-correlation. The results of this study's field data suggested that the conveyor belt noise was a wide band signal. At the same time, it was also found to have an intense time structure. The Green's function, which was retrieved using deconvolution interferometry, displayed a higher time resolution than those obtained by the cross-correlation. Finally, this study's field data illustrated that the conveyor belt noise could be potentially applied to monitor the stress variations around longwall mining panels. As a result, the proposed method was expected to be an effective method for the reduction of coal mine disasters.

KEY WORDS: coal working face, conveyer belt, seismic interferometry, noise imaging, passive source.

INTRODUCTION

Serious geological coal mine disasters are always accompanied by stress variations in the rock stratum. Therefore, the monitoring of the stress variations around the working faces of mines can be done indirectly using seismic wave

0963-0651/17/$5.00

velocity scanning, due to the close relationship between the stress and the wave velocity. The geological hazards of coal mining processes around working faces primarily include roof caving, gas outbursts, pressured water outbursts, and so on. Along with the coal mining processes, the extremely large overlying stratum could partly lose its support, and the original stress balance would thereby be broken (Jeremic, 1985). The cracks become gradually interconnected, and eventually lead to geological hazards. The working faces are the primary disaster zones, and the real-time stress monitoring of these areas is critical to ensuring work safety. Borehole stress meters are usually setup to measure stress changes. However, this method can only detect the stresses near the meters. At the same time, seismic wave transmission surveying makes it possible to investigate on a larger scale than the excavation zones. The wave velocity changes can be used to monitor the stress changes, due to the fact that the formation velocity is determined by the density and Young's modulus, and the latter is dependent on the variances of stress (Adams and Williamson, 1923). For cracks and pores to form, the changes in the wave velocity caused by stress changes would need to be remarkable, while the cracks and pores can also be easily deformed (Prasad and Maghnani, 1997; Cox, 1999). The wave velocities of both the seam roofs and floors can be monitored by body waves, which are transmitted in the roofs and floors, respectively. The velocities of the coal seams can be monitored by the In-Seam-Wave. Since the changes in the velocities are small, it is very important to fix the wave sources and recorders. The recorders can be easily mounted in fixed positions. However, the setting of repeatable sources is not that simple. Explosive sources are not applicable in these cases. Although hammering is a repeatable source, its energy is not intense. Therefore, it is very difficult to achieve long-term monitoring. The use of mining-induced micro seismic events as sources has also been previously proposed. However, the method displayed inaccuracies in the source locations, as well as inadequate ray path densities (Hosseini et al., 2011). Along with repetitive excitation in fixed locations, the sources must be safe for the mining equipment. Most importantly, it cannot disturb the normal mining operations. Therefore, the repeatable sources of conveyor belt noise were presented in this research study. Fig. 1 shows a common longwall working face. The coal was cut by a shearer, which had two cutting drums, and was then transported to a crusher by scraper conveyors. After the coal is reduced in size in a crusher, it is loaded onto a conveyor belt to be transported to the surface. The conveyor belts are installed in the belt tunnels, which are approximately 0.5 m from the coal mine walls. It was found to be extremely advantageous to use conveyor belts systems as wave sources for the following reasons: First of all, the sources were allocated at fixed positions; secondly, detecting the noise for long periods of time made it possible to obtain sufficient seismic energy, even if the power was weak. Despite all the advantages, the idea of using conveyor belts as seismic sources had never previously been proposed. This was possibly due to the fact that another notable passive source existed - the coal shearer.

In 1980, the idea of using coal shearers as seismic sources in channel wave exploration was proposed by Buchanan et al. (1980). However, the idea has not yet been implemented. In the mid-1990's, the United States Bureau of Mines attempted to use coal shearers as an energy sources for attenuation tomography (Westman and Haramy, 1996). In 2001, Taylor used a mine cutter as a seismic source in order to predict geological structures ahead of the machines (Taylor et al., 2001). A similar method, which was proposed by Poletto and Petronio (2006), involved tunnel seismic sources while drilling, which used the noise excited by tunnel boring machines. Luo et al. (2010) and King and Luo (2009), proposed the use of coal shearers as seismic sources, and tomographic imaging ahead of mining processes in 2009. A similar research study has also been carried out in China in recent years (Luo et al., 2001, 2013). In all of these studies, shearers were used as the conventional working drill source. Despite the fact that there have been some successful examples, the shearers have displayed some shortcomings as seismic sources as follows: First, the shearers move along the long walls. Therefore, the working faces are only partly covered by the seismic velocity rays; and second, under the conditions of loose coal, the energy of the shearers' noise can be relatively weak. These limitations may partly be overcome by the proposed conveyor belt sources, which are located in fixed positions, with energy levels which can be accumulated in long time windows. The conveyor belts are located in the belt tunnels from the beginning to the end of the mining processes, and the seismic

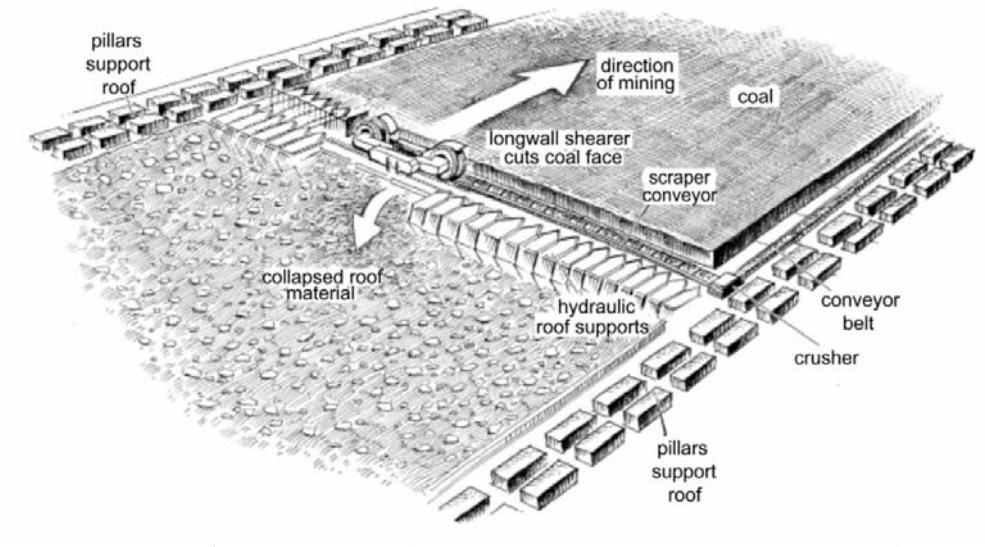

Fig. 1. Mining operation using longwall mining (Image courtesy of the United States Securities and Exchange Commission).

velocity rays can cover the entire working face. Therefore, based on seismic interferometry, the retrieval of Green's function from conveyor belt noise presented an exciting new field of study.

During the history of seismic interferometry, Claerbout demonstrated the methodology of Green's function retrieval for a 1D medium by autocorrelating traces generated by buried sources (Claerbout, 1968). Later, this method was extended to 3D media and referred to as daylight imaging (Rickett and Claerbout, 1999). In 2001, Schuster relaxed the restrictions of the random distribution sources, and renamed it "seismic interferometry" (Schuster, 2001). It was shown that, by applying a stationary phase approximation, the redatumed data obtained from a few regular distributed sources, could provide useful images of the reflectivity distributions. In 2002, Wapenaar et al. rigorously proved Claerbout's conjecture. They found that the related reciprocity equation of the correlation type was the mathematical basis for the correlation-based methods (Wapenaar et al., 2001). Although interferometry is typically done by correlations, it also can be accomplished by deconvolutions (Vasconcelos and Snieder, 2008) or cross-coherence (Nakata et al., 2001). These two methods are suitable for interferometry applications in which excitation is a complicated source-time function. Also, cross-coherence, which normalizes the spectral trace amplitude, is the preferred algorithm in the presence of highly variable and strong additive random noise.

The main underlying assumptions of these trace-by-trace methods are that the media are lossless and the wave fields are equipartitioned. These assumptions are often violated in practice, and the media of interest are often illuminated from one side only. These limitations may partly be overcome by reformulating the seismic interferometry as a multidimensional deconvolution (MDD) process (Wapenaar et al., 2008, 2011). However, in practical circumstances, the point-spread function cannot always be obtained from the field data, particularly when the detectors (as virtual sources) and passive sources are located in the same places.

It has been determined that there are some issues in using the energy of conveyor belt noise as seismic sources. First, the belt machines are regular thread sources, and therefore do not meet the equipartition illumination conditions. Second, the autocorrelation functions of the noise are complicated source-time functions with low resolution. Third, it has proven difficult to obtain the point spread functions, due to the fact that the conveyor belts and recorders almost coincide, and the MMD process is not applicable.

In this study, a stationary phase integration was proposed to analyze the energy of conveyor belt noise. In addition, both a numerical simulation and field data were applied to test its accuracy and potential application.

STATIONARY PHASE ANALYSIS

The working faces are rectangular coal seams which are surrounded by an air return tunnel, longwall face, and conveyor belt tunnel, as shown in Fig.2. The shearers work back and forth along the longwall faces. The longwall faces are approximately 300 m in length, and the lengths of the tunnels are approximately 500 m. The recorders are mounted at intervals of 10 m in the air return tunnels, and at 20 m intervals in the conveyor belt tunnels. The distances from the belts to the walls are usually 0.5 m, which was generally ignored in the analysis.

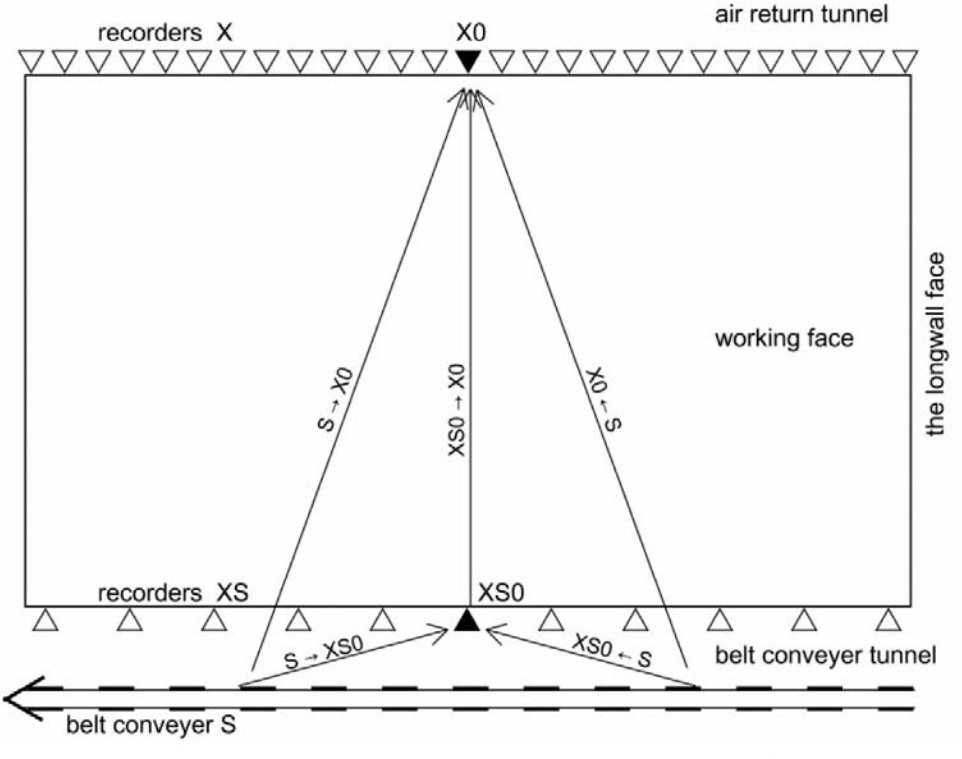

Fig. 2. Top view of a working face and the wave fields of conveyor belt noise. The triangles denote the receivers, and two special ones are denoted by solid triangles. The conveyor belt stood on the ground with discrete supports. There were three primary wave fields, two of which were real waves from conveyor belt S, and one was a virtual wave field (Calvert et al., 2004) from one receiver to another (XS0 → X0).

In this research study, the recorders were mounted on the bolt ends of the tunnel's wall in the experiments. In practical applications, the recorders can also be placed in the bases or roof rock seams in accordance with the purposes of observations. The conveyor belt was approximately 0.5 m from the coal wall, so that the near-field wave could also be recorded by belt tunnels' recorders. The energy of the conveyor belts' vibrations was more intense when the conveyor carried coal, especially when the belt joints crossed the supporting wheels. The intervals between the belt brackets were approximately 3 m. Due to the uniform spacing between the belt brackets, it was reasonable to consider the conveyor belt as a linear array of discrete sources.

In Fig. 2, S denotes the conveyor belt; XS denotes the recorders in the belt tunnel; and X denotes the recorders in air return tunnel. In order to facilitate the description, two special recorders are denoted as XS0 and X0, and are shown as solid triangles in the figure. Then, following the above notations, a stationary phase analysis was applied to the correlation functions of recorders XS0 and X0.

The acoustic reciprocity equation of the correlation type (Aki and Richards, 2002; Wapenaar, 2004) was as follows:

$$G(X0,XS0) - G(XS0,X0)^* = \oint_{Sur} [G(XS0,S)^* \partial_i G(X0,S) - G(X0,S)\partial_i G(XS0,S)] d^2x \quad , \qquad (1)$$

where G(X0,S) denotes Green's function from the discrete source S to the recorder X0; G(XS0,S) denotes Green's function from the discrete source S to the recorder XS0, G(XS0,X0) denotes Green's function from the recorder XS0 to X0; G(XS0,X0)* denotes the acausal part of G(X0,XS0); δ_i denotes the partial derivative in the x_i direction; and Einstein's summation convention is used for subscript i.

The retrieval of Green's function by cross-correlation had an underlying assumption that the recorders XS0 and S0 should be isotropically surrounded by discrete sources. However, in practice, the working face was illuminated from one side only, so the integration was only along the conveyor belt machine.

In the far-field approximation, eq. (1) could be simplified as (Schuster, 2009):

$$2jIm[G(X0,XS0)] \approx 2jk \oint_{belt} [G(XS0,S)^* G(X0,S)] dx \quad , \qquad (2)$$

where j denotes the imaginary unit and Im denotes the imaginary part, k denotes the wavenumber.

The stationary phase analysis was found to be simple due to the fact that only the direct wave was considered. Since the conveyor belt was simplified as a linear array of discrete sources, the right-hand side of eq. (2) could be simplified into an accumulation of many point sources. Not all of the energy of the discrete sources contributed to the retrieval of Green's function between XS0 and X0, unless the discrete sources were near the stationary phase points. This was due to the fact that the energy of other discrete sources was offset with each other, or partially came into spurious events. The phase of the correlation function in the integration of eq. (2) was the phase difference of the two Green's functions G(S → XS0) and G(S → S0), and in the time domain, it was the arrival-time difference (shown in Fig. 2). According to the principle of the three sides of the triangle, the arrival-time reached the maximum value when source S was on the extension of line XS0 → X0. As an example, Fig. 3 shows the three wave fields' arrival-times as a function of x, which were the discrete source points. The velocity was assumed to be 1000 m/s. The dashed dotted line denotes the arrival-time function for G(S → XS0), and the relational expression was as follows:

$$t = |x - 260m| \,/\, 1000(m/s) \quad , \tag{3}$$

where x is the coordinate along the belt S, and the recorder XS0 located at 260m. The dotted line denotes the arrival-time function for S → X0, its relational expression is

$$t = [(x - 260m)^2 + (300m)^2]^{1/2} \,/\, 1000(m/s) \quad . \tag{4}$$

The arrival-time function for the correlation function of XS0 and X0 is the difference of the two waves above

$$t = \{[(x - 260m)^2 + (300m)^2]^{1/2} - |x - 260m|\} \,/\, 1000(m/s) \quad , \tag{5}$$

it is shown as the solid line in Fig. 3.

The correlation function of XS0 and X0 is the convolution result from an accumulation, which is implemented with the expression (5) along the total belt discrete sources x. Fig. 4 shows a numerical case with the Ricker wavelet, the belt conveyer is approximated to a linear array of 51 sources. The rightmost trace is the correlation function of the 40-th trace at the two tunnels respectively, which is the superposition of all the traces left. Except for the sources near the 40-th trace, which is the stationary phase point of the accumulation, the other arrival-times are earlier. All of the spurious events arrive earlier than the true one. This feature is very useful.

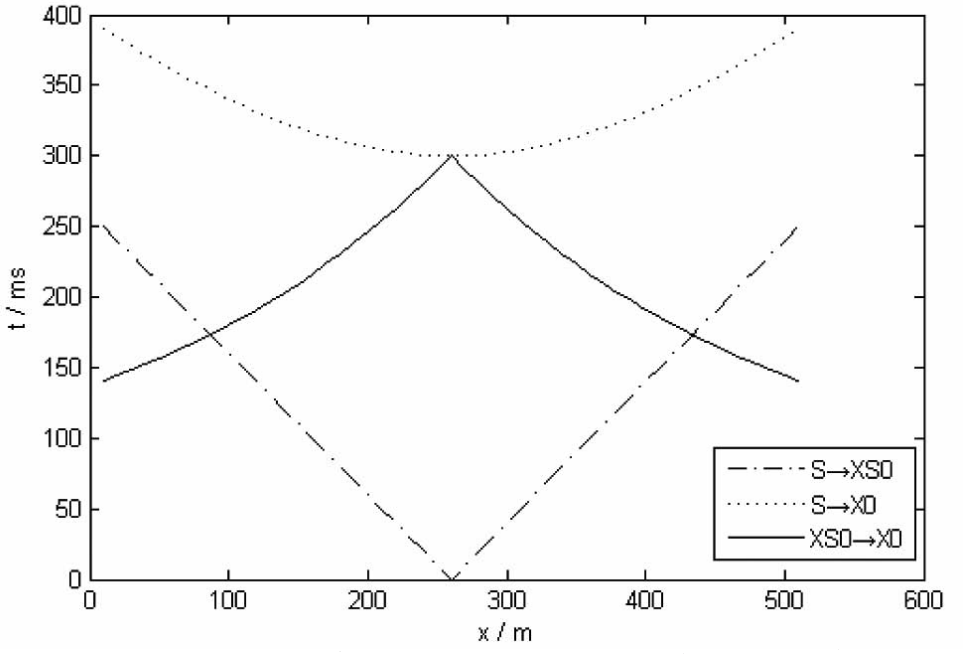

Fig. 3. Arrival-time functions for the discrete focal points in the conveyer belt. The two receivers, XS0 and X0, are at 260 m in the belt tunnel and the air return tunnel, respectively. The arrival-time functions for XS0 → X0 is the arrival-time difference for the other two wave fields.

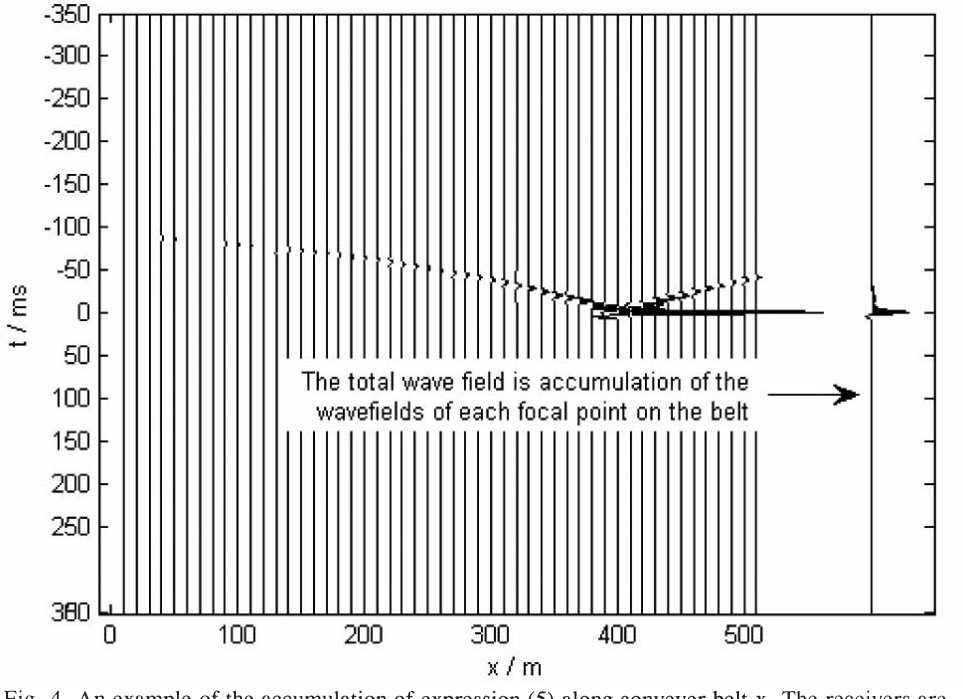

Fig. 4. An example of the accumulation of expression (5) along conveyer belt x. The receivers are at 400 m, and the traces for every focal point are show, the sum of the traces is the right most one.

Here we present an analysis of stationary phase integral for the wave field shown in Fig. 2. The Green's functions of S → XS0 and S → X0 are denoted respectively as

$$G_1(x) = 1/t_1(x) * e^{-\omega\varphi_1(x)} , \tag{6}$$

$$G_2(x) = 1/t_2(x) * e^{-\omega\varphi_2(x)} , \tag{7}$$

where $1/t_1$ and $1/t_2$ denote the diffusion attenuation, $\varphi_1(x)$ and $\varphi_2(x)$ denote the phases. The Green's function of XS0 → X0 is obtained from the cross-correlation of the two

$$G(x) = 1/[t_1(x)t_2(x)] * e^{-\omega[\varphi_2(x)-\varphi_1(x)]} . \tag{8}$$

The amplitude $g(x) = 1/[t_1(x)t_2(x)]$ is the product of amplitudes of S → XS0 and S → X0. The phase $\varphi(x) = \varphi_2(x) - \varphi_1(x)$ is the phase difference of G(S → XS0) and G(S → X0). The real parts of the Green's function in eq. (8) are for the ω shifting from 50 to 450 Hz shown in Fig. 5. The $e^{-\omega[\varphi_2(x)-\varphi_1(x)]}$ is a rapidly oscillating function with total algebraic area going to zero as ω is increasing, except for the middle section of the stationary region. Accumulating along x, the values of five ω are shown in Fig. 6. The positive values of the integration define the half width of the Fresnel zone at the left of the original point. The higher the frequency, the narrower the Fresnel zone. It indicates that the low frequency energy is enhanced in the process.

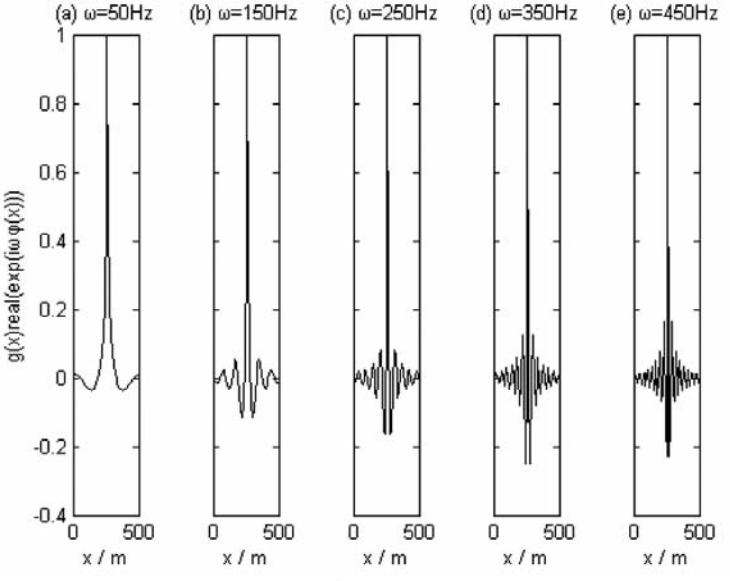

Fig. 5. The exponential function in expression (8) with five different frequencies. The higher the frequency, the smaller the algebraic area is.

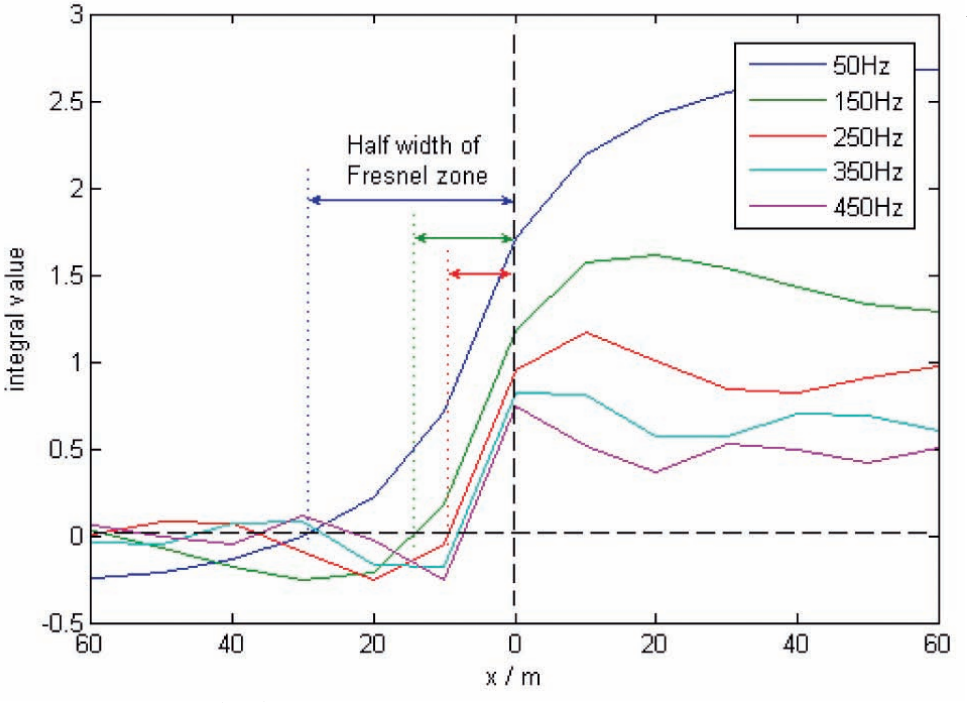

Fig. 6. Results for the accumulation of expression (8) of five different frequencies. The positive range of x is the Fresnel zones, and the lower frequency component have a wider Fresnel zone, and its integral quantity is also larger.

NUMERICAL RESULTS

The modeled noise response was obtained by the convolution of the Green's functions with the wavelet-white noises in expressions (6) and (7). Although there are correlated components in practice, the white noises from the source points were uncorrelated in this study's simulation. As detailed in Fig.2, the working face length was 500 m, and spacing of the recorders was 10 m. There were 51 recorders in each tunnel. The conveyor belt was approximated to 51 discrete sources, and the interval was also 10 m. In the model, the space between the conveyor belt and the wall was ignored. Every trace was obtained by the accumulation of the responses from all of the sources in the conveyor belt. Fig. 7(a) details the traces in the belt tunnel, and Fig. 7(b) shows the traces in the return air tunnel. The cross-correlation of the middle (26th) traces in the two tunnels is shown in Fig. 8. The event indicated the strongest energy

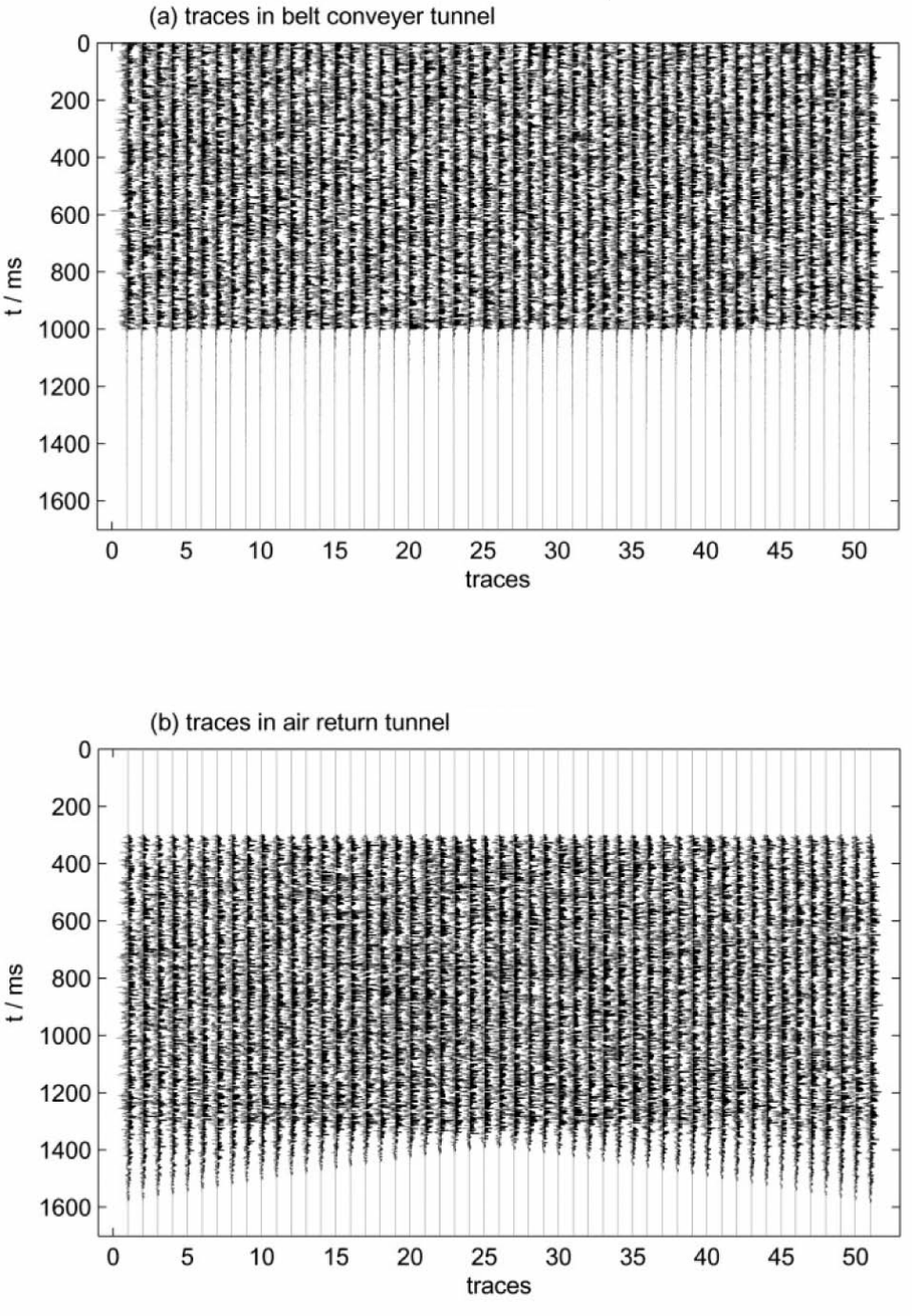

Fig. 7. The modeled noise responses in the belt tunnel (a) and air return tunnel (b). The noise at every focal point is uncorrelated with each other, and the length of noise is 1000 ms.

accords with the Green's function from point XS0 to X0. Other earlier weak events were considered to be spurious artifacts. The conclusion of the numerical simulation was found to be consistent with the previous theoretical analysis. It was clear that although the Green's function retrieved by the correlation method displayed some spurious events, these events could be easily distinguished by their earlier arrival-times.

For the noise sources, the point-spread function (PSF) was given by $\Gamma(XS,XS0,t) = \langle u^{in}(XS,t) * u^{in}(XS0,-t)\rangle$; the superscripts "in" denote the inward-propagating waves; and $\langle\cdot\rangle$ denotes the ensemble averaging. When the inward propagating waves could not be separated, the PSF was obtained from correlation function $C(XS,XS0,t) = \langle u(XS,t) * u(XS0,-t)\rangle$ by time-windowing (Wapenaar et al., 2011). However, as virtual sources, the recorders in the proposed method were arranged in the belt tunnel, and the correlation function C(XS,XS0,t) was found to be severely polluted by noise. The exception was the auto-correlation, as shown in Fig. 9. Due to the fact that the PSF could not be obtained from the practical data, the retrieval of Green's function from the MDD method remained a pending problem. Therefore, it was concluded that the trace-by-trace interferometry was an acceptable method, which included cross-correlation, deconvolution, and cross-coherence.

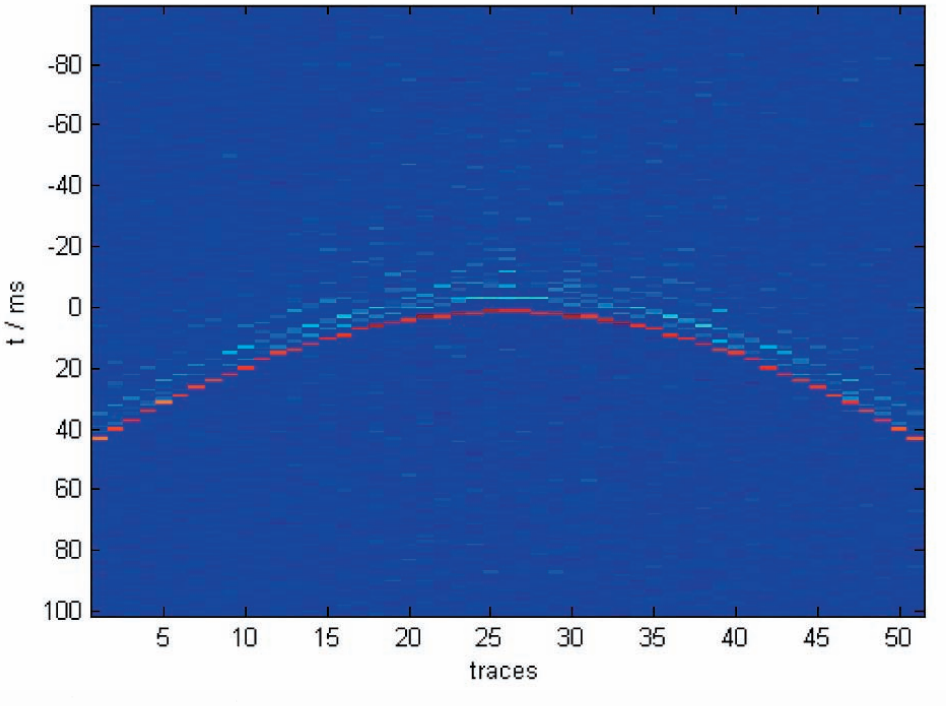

Fig. 8. The correlation interferometry of the traces in the air return tunnel and the 26-th trace in the belt tunnel. The strongest event (in red) is the 'virtual shot gather', and the earlier events are spurious artifacts.

FIELD DATA RESULTS

In this study's numerical analysis, the theoretical wavelet with white noise had sharp pulse-like autocorrelation functions, as well as the highest time resolution. However, for the field data, this was not the case. The noise of conveyor belt was emitted from the rotators, running belt, and impacting belt connectors (Fig. 10). The belt was very taut, and pulled quickly when carrying coal. Therefore, the energy of the vibration noise was relatively high. The noise was a mix of periodic waves and white noise. The periodic components came from the rotators, while the white component was created by the impact. Since all the brackets were connected by a beam and belt, it was found that the vibrations of the brackets were not completely uncorrelated.

Fig. 11(a) shows a set of conveyor belt noise. The traces which were seen were found to be different from each other. The amplitude spectrum of each trace is detailed in Fig. 11(b). The energy of the noise was primarily distributed in a frequency range of 50 to 250 Hz. A 50 Hz power line occurred due to the lighting and electrical equipment in the tunnel. It was determined that, regardless of whether it was in the time domain or in the frequency domain, a

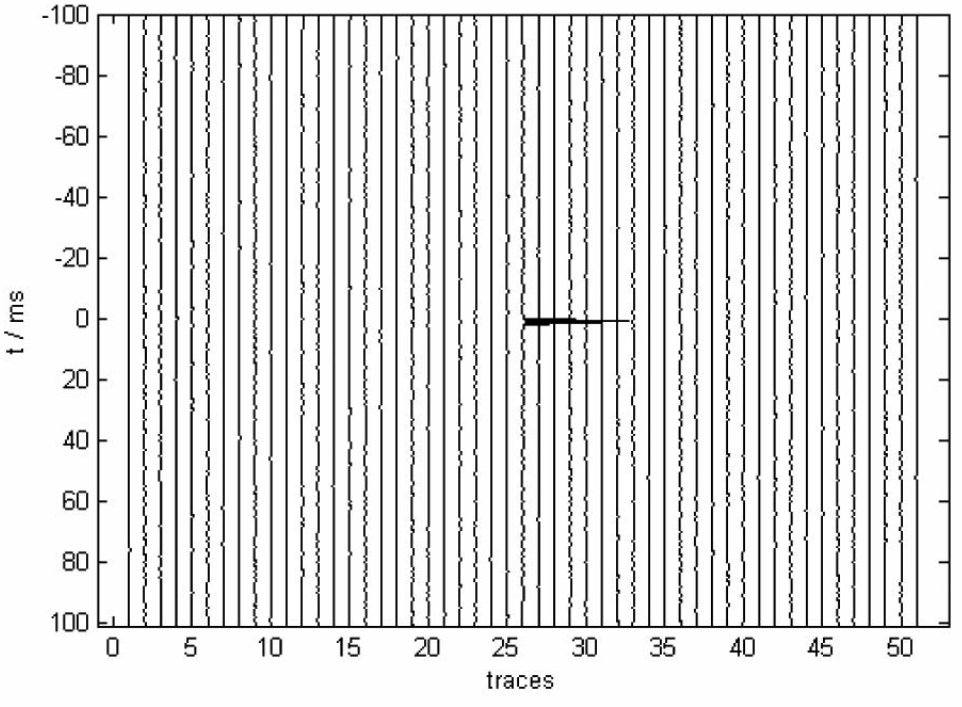

Fig. 9. The correlation functions C(XS,XS0,t), from which the PSF should be obtained. The correlation functions were immersed in white noise, except for the autocorrelation function.

strong time structure was clearly discernible. For this type of data, cross-correlation interferometry was not suitable for the relatively large side lobe of the correlation function, which would have reduced the space resolution dramatically. However, deconvolution interferometry was determined to be valid for these types of sources.

Fig. 10. The conveyer belt. The space between brackets is about 3 m.

Cross-correlation interferometry in the frequency domain is defined as

$$C = |W(s)|^2 G(XS0,S)*G(X0,S) \quad , \tag{6}$$

where $|W(s)|^2$ denotes auto-correlation of the source function.

The frequency domain of the deconvolution is represented as (Vasconcelos and Snieder, 2008):

$$\begin{aligned} D &= |W(s)|^2 G(XS0,S)*G(X0,S)/|W(s)|^2|G(XS0,S)|^2 \\ &= G(XS0,S)*G(X0,S)/|G(XS0,S)|^2 \quad . \end{aligned} \tag{7}$$

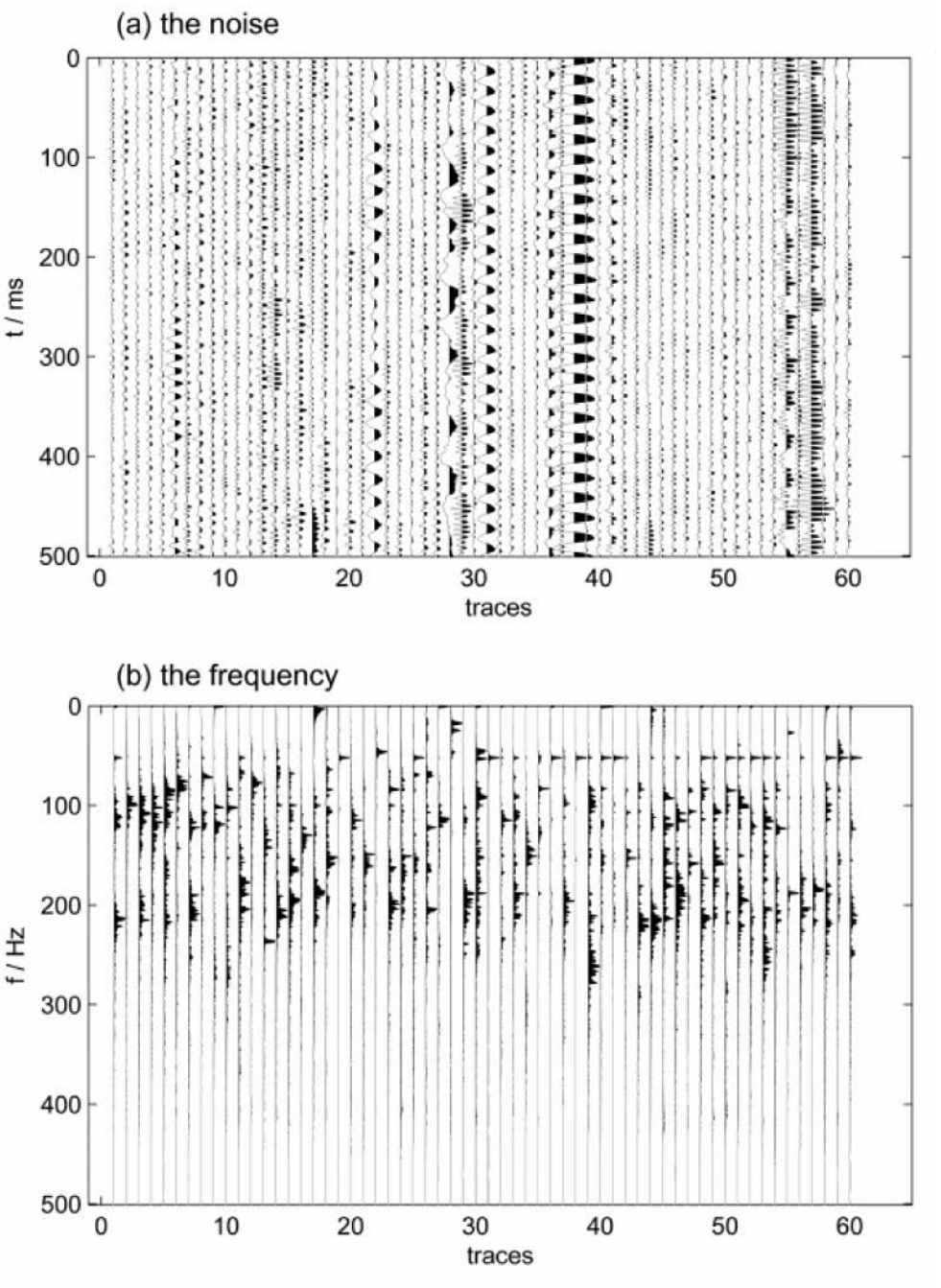

Fig. 11. The field data of the conveyer belt's noise (a) and its frequency (b). The data is recorded along the belt, and the space between the recorders is 10 m.

The auto-correlation of source time function $|W(s)|^2$ can be eliminated in the process of deconvolution. To avoid instabilities when the denominator is zero or close to zero, the addition of a small percentage of white noise (or positive term) at the denominator is beneficial.

There are several deconvolution algorithms, and the simplest one is the 'water level' deconvolution (Clayton and Wiggins, 1967):

$$D = G(XS0,S)*G(X0,S)/[|G(XS0,S)|^2 + \varepsilon\langle|G(XS0,S)|^2\rangle] , \quad (8)$$

where $\langle\cdot\rangle$ denotes average value. The factor ε is a free-parameter that we choose by visually inspecting the output of the deconvolution. 'Water level' deconvolution is simple and fast to execute.

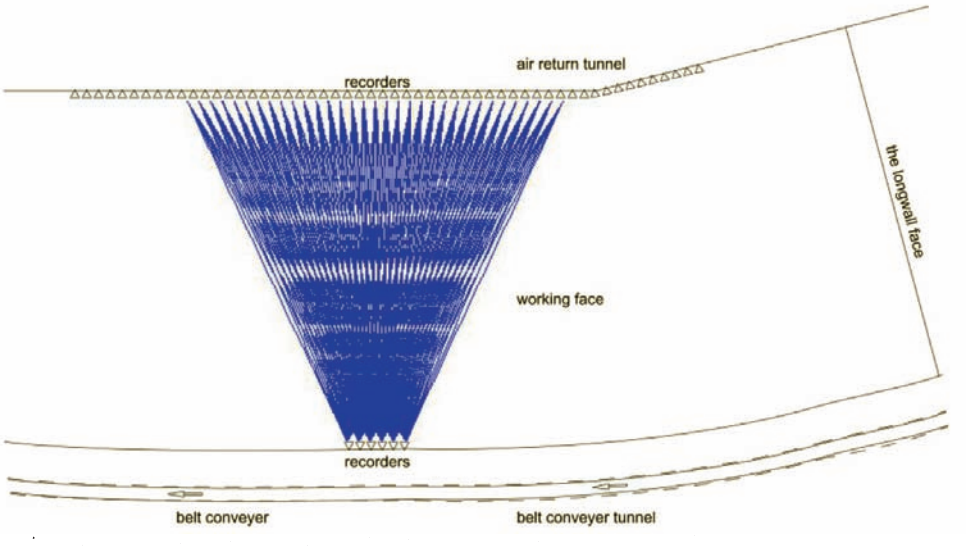

Fig. 12. An actual working face and the rays (in blue lines). Some traces in the air return tunnel were abandoned due to low S/N ratios.

Fig. 12 shows an actual working face, where 74 recorders were located along an air return tunnel, and six were located along a belt tunnel. All of the space intervals between the recorders were 10 m. Two experiments were carried out at a time interval of 24 hours, and 8 hours of data was acquired in each experiment. As indicated in the figure, the area covered by the seismic rays (blue lines) was the study region. Only 54 traces were selected in the return air tunnel due to their high s/n ratios. Among these, 20 recorders were found to be located too far away to determine the accurate travel time. The coal shearer's noise was found to be a strong disturbance when considering the energy of the conveyor belt. The coal shearer had two types of jobs, namely cutting and pushing the coal. The energy of noise was very intense during the coal cutting stage, but is weaker during the coal pushing stage. In this study, in order to avoid the disturbances, the data was selected at the times when the conveyor belt was working, and the coal shearer was not cutting. During this study's processing, 15 minutes of data which met the conditions were selected.

Fig. 13(a) shows the "virtual shot gathers" obtained from the correlation interferometry using a 60 Hz low pass filter. Fig. 13(b) details the results of the deconvolution interferometry. The 1 to 6 traces were those in the belt tunnel, and the rest were in the return air tunnel. The correlation interferometry results were blurred by the complex wavelet. It was obvious that the time structure of the conveyor belt noise was very strong, and the wavelet side lobe was too large. In contrast to the correlation interferometry, the corresponding deconvolution interferometry results were found to be very good. This was due to the fact that the time structure had been reduced. The magnitude spectra of the virtual shot gathers are shown in Fig. 14. The correlation interferometry spectrum contained periodic events from the power line (shown in Fig. 14a). The deconvolution gathers had a wider band, and the periodic events were reduced (shown in Fig. 14b). In this study, only the S wave was analyzed. This was due to the fact that the S wave energy was very intense in the coal seam, and its frequency band was relatively low. The P wave was found to be too weak to achieve high quality results. The energy of the In-Seam wave was also relatively strong. However, it was determined to be more suitable for structural prospecting than the detection of rock stress changes.

By using the six traces in the belt tunnel as the virtual shots, the virtual shot gathering was obtained by the deconvolution interferometry. The ray coverage of the working surface is shown in Fig. 12. The two seismic tomographies of the coverage working face were generated using the travel time of rays (Fig. 15). The time interval of the two experiments was 24 hours, and the longwall face moved forward 8 m. The two images were determined to be similar since the longwall face was far from the imaging area. However, there were some differences observed between the two images near the traces in the belt tunnel. This was mainly due to the fact that the information scarcity for the 1 to 3 traces were damaged during the second test.

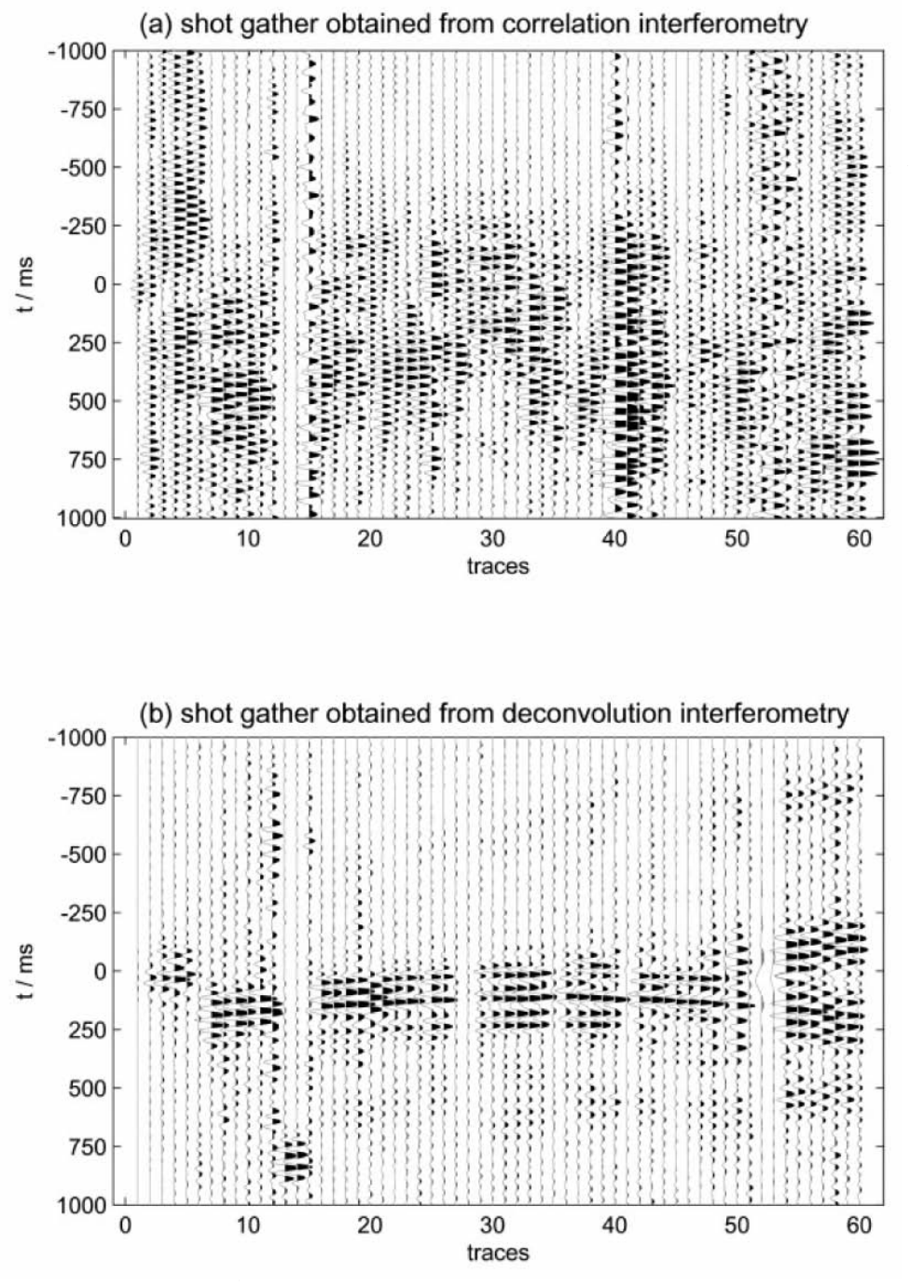

Fig. 13. Virtual shot gathers generated from: (a) the correlation interferometry; and (b) the deconvolution interferometry.

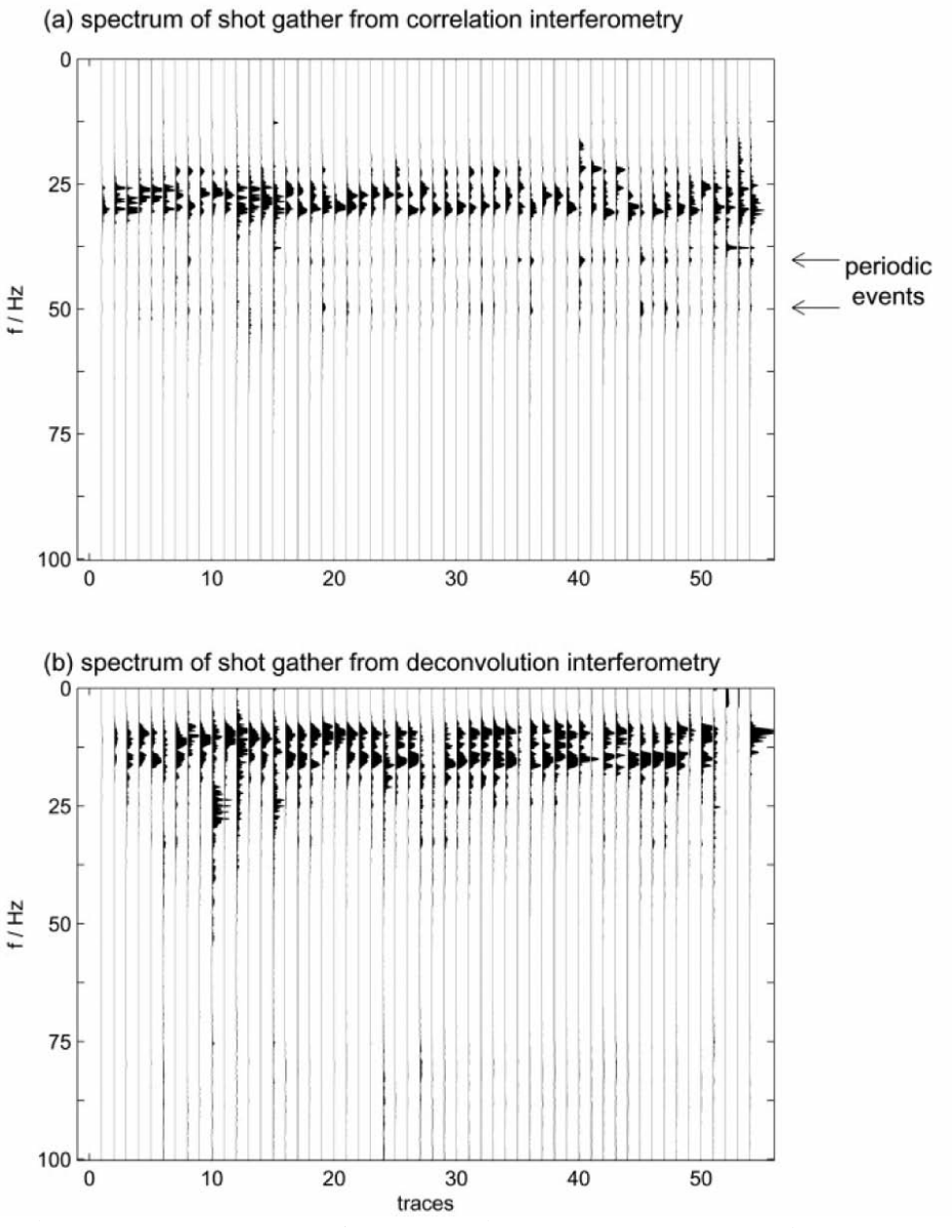

Fig. 14. Spectra of the virtual shot gathers: (a) correlation gathers; (b) deconvolution gathers.

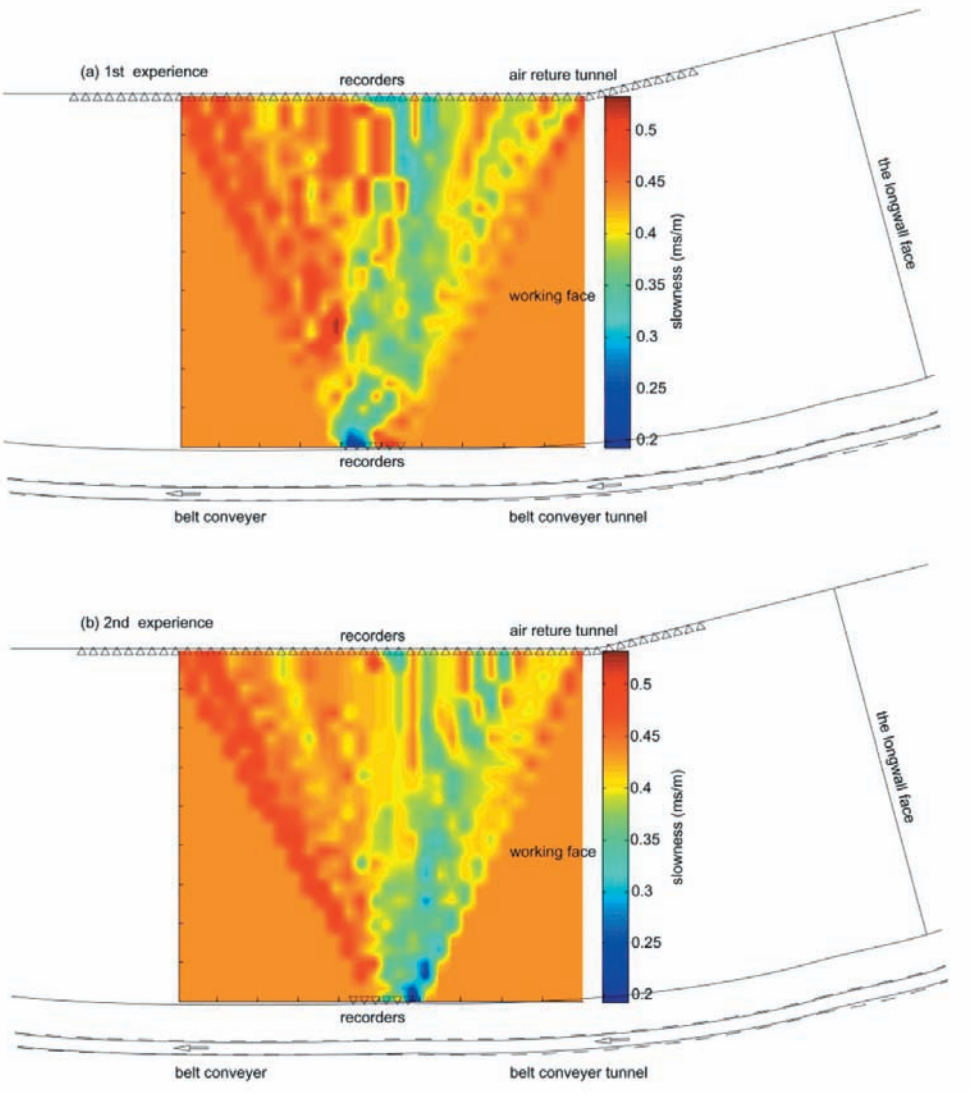

Fig. 15. Seismic tomography of the area covered by rays in the working face. Two experiments were conducted at intervals of 24 hours. The 1 to 3 recorders in the belt tunnel were damaged during the second experience, which resulted in uncertainty near the belt tunnel.

CONCLUSIONS

In this study, a method of using the energy from conveyor belt vibrations to image the working face ahead of mining operations was proposed. It was demonstrated that the conveyor belt induced seismic waves could be observed

beyond several hundred meters. Meanwhile, the conveyor belt noise could be cross-correlated across pairs of geophones to yield relative traveltimes, which could then be inverted for wave velocities. Since seismic velocity varies with the rock stress, it was possible to conduct stress monitoring of the rock masses from these images. The advantages of using conveyor belts as seismic sources were that they are in fixed positions, and their noise energy can be accumulated in long time windows.

This study revealed how to use the noise from conveyor belts to generate traveltime information. The key requirement was that the conveyor belts acted as a linear array source, and did not meet the conditions of equipartition of the wave field. Also, there were spurious events observed in the interference results. In addition, since the PSF could not be obtained from the practical data, MMD was not an option to retrieve the Green's function. Both the stationary phase analysis and the numerical simulation suggested that the spurious events had shorter arrival-times. Therefore, the Green's function could be retrieved by trace-to-trace seismic interferometry.

In addition, due to the complicated source-time function, it was determined that interferometry by deconvolution was particularly important for recovering the impulse responses. The interferometry by deconvolution yielded wide-band images from the conveyor belt noise without requiring an independent estimation of the belt's excitation. Meanwhile, by using the multi-dimensional deconvolution interferometry, the problems of one-side illumination could be solved. However, it was difficult to obtain the point spread function in the field data.

ACKNOWLEDGMENTS

This research project was funded by the China National Science and Technology Major Projects (2011ZX05040-002), and the China Postdoctoral Science Foundation Funded Project (2012M511967). The authors would like to express their gratitude to the Fu Cheng Coal Mine for their support during this experimental study.

REFERENCES

Adams, L.H. and Williamson, E.D., 1923. On the compressibility of minerals and rocks at high pressures. J. Franklin Inst., 195: 475-531.

Aki, K. and Richards, P.G., 2002. Quantitative Seismology. Freeman & Co, New York.

Buchanan, D.J., Mason, I. and Davis, R., 1980. The coal cutter as a seismic source in channel wave exploration. IEEE Transact. Geosci. Remote Sens., GE-18: 318-320.

Calvert, R.W., Bakulin, A. and Jones, T.C., 2004. Virtual sources, a new way to remove overburden problems. Extended Abstr., 66th EAGE Conf., Paris: P234.

Claerbout, J.F., 1968. Synthesis of a layered medium from its acoustic transmission response. Geophysics, 33: 264-269.

Clayton, R.W. and Wiggins, R.A., 1967. Source shape estimation and deconvolution of teleseismic body waves. Geophys. J. Roy. Astr. Soc., 47: 151-177.

Cox, M.,1999. Static Corrections for Seismic Reflection Surveys. SEG, Tulsa, OK.

Hosseini, N., Oraee, K., Shahriar, K. and Goshtasbi, K., 2011. Studying the stress redistribution around the longwall mining panel using passive seismic velocity tomography and geostatistical estimation. Arab. J. Geosci., 6: 1407-1416.

Jeremic, M.L., 1985. Strata Mechanics in Coal Mining. Taylor & Francis Group, London.

King, A. and Luo, X., 2009. Methodology for tomographic imaging ahead of mining using the cutter as a seismic source. Geophysics, 74(2): M1-M8.

Lu, B., Cheng, J.Y. and Hu, J.W., 2001. Seismic features of vibration induced by mining machines and feasibility to be seismic sources. Proc. Earth Planet. Sci., 3: 76-85.

Lu, B., Cheng, J.Y. and Hu, J.W., 2013. Cutter source signal extraction and preliminary application. J. Chin. Coal Soc., (in Chinese), 38: 2202-2207.

Luo, X., King, A. and van de Werken, M., 2009. Tomographic imaging of rock conditions ahead of mining using the cutter as a seismic source-a feasibility study. IEEE Transact. Geosci. Remote Sens., 47: 3671-3678.

Nakata, N., Snieder, R. and Tsuji, T., 2011. Shear wave imaging from traffic noise using seismic interferometry by cross-coherence. Geophysics, 76(6): SA97-SA106.

Poletto, F. and Petronio, L., 2006. Seismic interferometry with a TBM source of transmitted and reflected waves. Geophysics, 71(4): SI85-SI93.

Prasad, M. and Manghnani, M.H., 1997. Effects of pore and differential pressure on compressional wave velocity and quality factor in Berea and Michigan sandstones. Geophysics, 62(4): 1163-1176.

Rickett, J. and Claerbout, J.F., 1999. Acoustic daylight imaging via spectral factorization: Helioseismology and reservoir monitoring. The Leading Edge, 18: 957-960.

Schuster, G.T., 2001. Seismic interferometric/daylight imaging: Tutorial. Extended Abstr., 63rd EAGE Conf., Amsterdam.

Schuster, G.T., 2009. Seismic Interferometry. Cambridge University Press, Cambridge.

Taylor, N., Merriam, J. and Gendzwill, D., 2001. The mining machine as a seismic source for in-seam reflection mapping. Expanded Abstr., 71st Ann. Internat. SEG Mtg., San Antonio: 1365-1368.

Vasconcelos, I. and Snieder, R., 2008. Interferometry by deconvolution: Part 2 - Theory for elastic waves and application to drill-bit seismic imaging. Geophysics, 73(3): S129-S141.

Wapenaar, K., Draganov, D., Thorbecke, J. and Fokkema, J., 2002. Theory of acoustic daylight imaging revisited. Expanded Abstr., 72nd Ann. Internat. SEG Mtg., Salt Lake City: 2269-2272.

Wapenaar, K., 2004. Retrieving the elastodynamic Green's function of an arbitrary inhomogeneous medium by cross correlation. Phys. Rev. Lett., 93: 254301-1-4.

Wapenaar, K., van der Neut, J. and Ruigrok, E., 2008. Passive seismic interferometry by multidimensional deconvolution. Geophysics, 73(6): A51-A56.

Wapenaar, K., van der Neut, J. and Ruigrok, E., 2011. Seismic interferometry by crosscorrelation and by multi-dimensional deconvolution: a systematic comparison. Geoph. J. Internat., 185: 1335-1364.

Westman, E.C. and Haramy, K.Y., 1996. Rock A D. Seismic tomography for longwall stress analysis. Proc. 2nd North Am. Rock Mech. Symp., Montreal, QC: 397-403.